Available online at www.CivileJournal.org

Civil Engineering Journal

Vol. 4, No. 11, November, 2018

Analytical Assessment of Bending Ductility in FRP Strengthened RHSC Beams

H. Ebrahimpour Komleh [a*], A.A. Maghsoudi [a]

[a] *Department of Civil Engineering, Faculty of Engineering, Shahid Bahonar University of Kerman, Kerman, Iran.*

Received 4 July 2018; Accepted 06 October 2018

Abstract

Over the past few years, a wide use of externally-bonded fiber-reinforced polymer composites (EB-FRP), for rehabilitation, strengthening and repair of existing/deteriorated reinforced/prestressed-concrete (RC/PC) structures has been observed. This paper presents a nonlinear iterative analytical approach conducted to investigate the effects of concrete strength, steel-reinforcement ratio and externally-reinforcement (FRP) stiffness on the flexural behavior and the curvature ductility index of the FRP-strengthened reinforced high-strength concrete (RHSC) beams. Analysis results using the proposed technique have shown very good agreement with the experimental data of FRP-strengthened/non-strengthened RHSC beams, regarding moment–curvature response, ultimate moment and failure mode. Also, a newly prediction equation for the curvature ductility index of FRP strengthened RHSC beams has been developed and verified. Then, converting equation of the curvature ductility index to energy one is proposed. Results indicate that the proposed predictions for the curvature and energy ductility indices are accurate to within 1.87% and 3.03% error for practical applications, respectively. Finally, limit values for these bending ductility indices, based on different design codes' criterion, are assessed and discussed.

Keywords: High Strength Concrete; FRP Composites; Nonlinear Analytical Model; Moment-Curvature Response; Ductility.

1. Introduction

Over the past three decades, rehabilitation, strengthening and repair of reinforced and prestressed concrete structures (RC, PC) by the external-bonding of fiber-reinforced polymer (EB-FRP) strips/sheets have become very popular around the world due to lots of interested advantages of FRP composites over other conventional materials. Consequently, numerous experimental/theoretical studies have been conducted to investigate the behavior of FRP-strengthened RC/PC members including beams, slabs, columns, shear walls and beam-column joints [1-10].

A vast number of failure mechanisms for RC beams strengthened with FRP strips/sheets have been experimentally reported [3, 9, 11]. Generally, these mechanisms can be categorized into three main types of flexural, shear and debonding failures. Debonding, as the most probable failure mode, is usually abrupt and uneconomical, and takes place by plate separation of the concrete surface before attaining the flexural capacity of the RC beam (while neither of the concrete or FRP are damage separately). In such a case the structural member is unemployable anymore and results in incomplete exploitation of the reinforcing FRP sheet.

Recently, concrete technology advancements have led to commercial production and widespread use of high-strength concrete (HSC), which has better durability and strength characteristics than normal-strength concrete (NSC) [12-13]. In ACI 363R (2010), HSC has a specified compressive strength of 55 MPa or greater [12].

* Corresponding author: h.ebrahimpourkomleh@eng.uk.ac.ir

http://dx.doi.org/10.28991/cej-03091194

Although the use of HSC in multi-storey buildings and bridges led to superior performance and economy, but due to its very high compression strength, HSC produces less ductile structural responses. Therefore, in seismic areas, ductility is an important factor in seismic design/rehabilitation of HSC members (especially FRP strengthened ones) under flexure.

Ductility of a structural member may be expressed as curvature ratio, rotation ratio, displacement ratio, and absorbed energy ratio [14-15]. In the case of a flexural member, cross-sectional ductility based on curvature is usually considered [16]. Assessment of the curvature ductility in FRP-strengthened RC beam sections has been the subject of few researches for recent two decades. Lee et al. (2004) developed an analytical solution for determining the allowable plate area to achieve a targeted value of ductility in RC beams retrofitted with FRP plates. Finally, based on regression analysis, they presented a simplified version of the method to relate the curvature ductility to the FRP plate ratio [17].

In 2006, Matthys and Taerwe reported a ductility index, in the form of the ultimate strengthened curvature to unstrengthened yield curvature ratio, based on an evaluation of ductility requirements in some design guidelines and by providing a parametric analysis on behavior of FRP-strengthened concrete members. By increasing amounts of CFRP, a trend of increasing strength and decreasing ductility was found. They concluded that the ductility of FRP-strengthened flexural members should be considered with care, as reduced deformability is obtained at ultimate [18].

Yost and Steffen (2014) provided a parametric analysis of strength and energy for unstrengthened/FRP-strengthened flexural NSC/HSC members at the service, yield, and ultimate limit states. Results showed that ductility in the form of ultimate-to-yield energy ratio was nonlinear, inversely related to the CFRP and steel reinforcement ratios, and trends differently at low versus moderate levels of CFRP reinforcement. For low amounts of steel and high amounts of CFRP, ductility decreases significantly relative to the unstrengthened condition [19].

Cross-sectional analyze as an easy and adopted methodology for design and assessment of flexural behavior in FRP-strengthened members, has been used by many researchers [1, 4, 17, 20-23]. An et al. (1991) have formed the basic analytical approach for assessment of stresses and deformations in rectangular/T-beam sections externally-reinforced with epoxy-bonded FRP plates [21]. In 2000, El-Mihily and Tedesco have presented a procedure for evaluating the ultimate capacity of strengthened RC beams based on crushing of concrete or FRP rupture [22].

In 2006, Toutanji et al. presented an analytical model for derivation of the moment–deflection response of simple-RC beams strengthened with FRP sheets, based on limit points of cracking, yielding of steel reinforcement and ultimate state of failure [23]. Akbarzadeh and Maghsoudi (2010) developed an analytical model to predict the load capacity and the flexural behavior of FRP-strengthened continuous reinforced high-strength concrete (RHSC) beams. According to obtained HSC experimental results, they neglected the falling branch of HSC stress–strain curve by assuming the strain in the maximum stress as the ultimate strain [4]. It could be noted that, between the above-mentioned models, premature debonding of FRP laminates was only considered in analytical models of Toutanji et al. (2006) and Akbarzadeh and Maghsoudi (2010).

In 2015, Skuturna and Valivonis performed a statistical analysis of the design methods (e.g. ACI440.2R-08, fib bulletin 14, TR55) to calculate the load-carrying capacity of RC flexural elements strengthened with external CFRP reinforcement, based on the experimental results of 80 beams. In most cases, obtained results statistically significantly differed from the experimental ones if calculated according to the fib and TR55 methodology. Also, the calculated values of the coefficient of confidence showed that the calculation results of the load-carrying capacity were more accurate when calculated according to ACI recommendations [24].

This research work addresses the following main objectives. The first is to examine the effects of concrete strength, steel-reinforcement ratio and externally-reinforcement (FRP) stiffness on the flexural behavior and the curvature ductility index of the FRP-strengthened RHSC beams. For this purpose, an iterative analytical technique is presented which considers: a) nonlinear behavior of materials by using basic models for complete pre- and post-peak stress-strain behavior of HSC and internal/external reinforcement (steel/FRP); b) occurrence possibility of FRP premature debonding mode. The second is to develop and verify newly prediction equations for curvature ductility and flexural energy ductility indices of FRP-strengthened RHSC beams. Also, according to obtained results, limit values for bending ductility indices, based on codes' ductility criterion, are assessed and discussed.

2. Analytical Model

The methodology adopted for the iterative analytical model is based on Akbarzadeh and Maghsoudi's model [4]. This model (Figure 1), takes into consideration the principles of strain compatibility and static equilibrium, and uses the defined constitutive relations for the HSC, steel and FRP to predict bending response. Assumptions for this approach are: i) plane sections remain plane after bending, ii) perfect bond exists between HSC and steel-reinforcement/FRP plates, iii) after cracking, the tensile stress in HSC may be neglected, iv) failure occurs when either ε_c reaches ε_{cu}, or ε_f reaches ε_{fd}.

Figure 2 presents a typical flexural response of strengthened beam, as the result of the analytical model. In this approach, the moment–curvature response is idealized as a nonlinear curve divided into three zones: 1) the first stage extends to the onset point of the concrete cracking; 2) the second one follows until the first yielding of the tensile steel reinforcement; 3) the last part continues until the failure point.

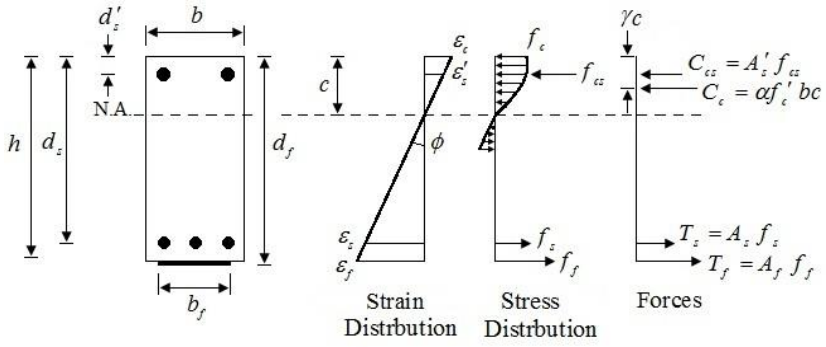

Figure 1. Strain, stress and force used in the moment–curvature model

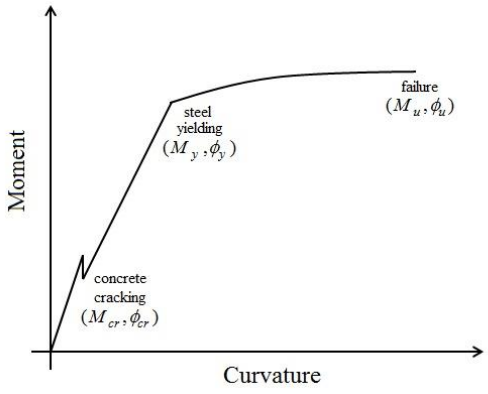

Figure 2. Moment–curvature response of strengthened beam

2.1. Material Properties

The applied nonlinear stress-strain models for HSC and steel-reinforcement, and elastic stress-strain relationship for FRP are described as following:

a) FRP

In FRP-strengthened RC beams, different failure modes have been observed. Specific failures of FRP plate are defined by rupture and premature debonding. Guidelines and codes (e.g. ACI 440.2R), suggested different models in order to predict debonding failure [1, 20, 25]. FRP materials are assumed to behave linearly elastic until failure. Based on ACI 440.2R (2017) recommendations, ε_{fe} is limited to the strain level at which debonding may occur, ε_{fd} , as defined in Equation 1 [25].

$$\varepsilon_{fd} = 0.41\sqrt{\frac{f_c'}{n_f E_f t_f}} \leq 0.9\varepsilon_{fu} \quad (1)$$

b) Steel-Reinforcement

The stress-strain relationship for steel-reinforcement is assumed to be bilinear, including elastic stage up to f_y, followed by linear hardening up to f_u.

c) HSC

The stress distribution of HSC in the compression zone is found from its stress–strain relationship. High performance-high strength concrete (HPHSC) specimens are generally more brittle than NSC. Therefore, at the ultimate stress state, they could be fractured suddenly under uniaxial compression. Collins and Porasz (1989), based on modifications to the work of Thorenfeldt et al. (1987) [26], and Popovics (1973) [27], suggested Equation 2 for stress–strain relationship of HSC [28].

$$f_c = f_c'\left(\frac{\varepsilon_c}{\varepsilon_0}\right)\left(\frac{n}{n-1+\left(\frac{\varepsilon_c}{\varepsilon_0}\right)^{nk}}\right) \quad (2)$$

Where $n = 0.8 + (f_c'/17)$, and the parameter k equals 1 for the ascending branch and $k = 0.67 + (f_c'/62)$ for the descending branch. For this curve, the strain at the peak stress is estimated as $\varepsilon_0 = (f_c'/E_c)n/(n-1)$, in which $E_c = 3320\sqrt{f_c'} + 6900$. Also the value of ε_{cu}, is assumed to be equal to 0.0035 [29].

Since the real stress distribution in compressive area at a cross section may be complex as well as variable, and also the area of stress distribution and its' center of gravity are more important than the geometry of the stress distribution for equilibrium equation; therefore, in this study, an equivalent rectangular compressive stress block model is used which suggested by building codes such as ACI 318 [30]. The main parameters for the equivalent stress block are stress and centroid factors (α and γ, respectively), as shown in Figure 1. As described in [4], these parameters are calculated as follow:

$$\alpha = \frac{\int_0^{\varepsilon_c} f_c \, d\varepsilon_c}{f_c' \, \varepsilon_c} \tag{3}$$

$$\gamma = 1 - \frac{\int_0^{\varepsilon_c} f_c \, \varepsilon_c \, d\varepsilon_c}{\varepsilon_c \int_0^{\varepsilon_c} f_c \, d\varepsilon_c} \tag{4}$$

Figure 3a and b show a plot of parameters α and γ as a function of HSC strain in extreme compression fiber ε_c, for different HSC strengths ranged between 60 to 100 MPa, respectively. The parameters α and γ, decrease with increasing HSC compression strength.

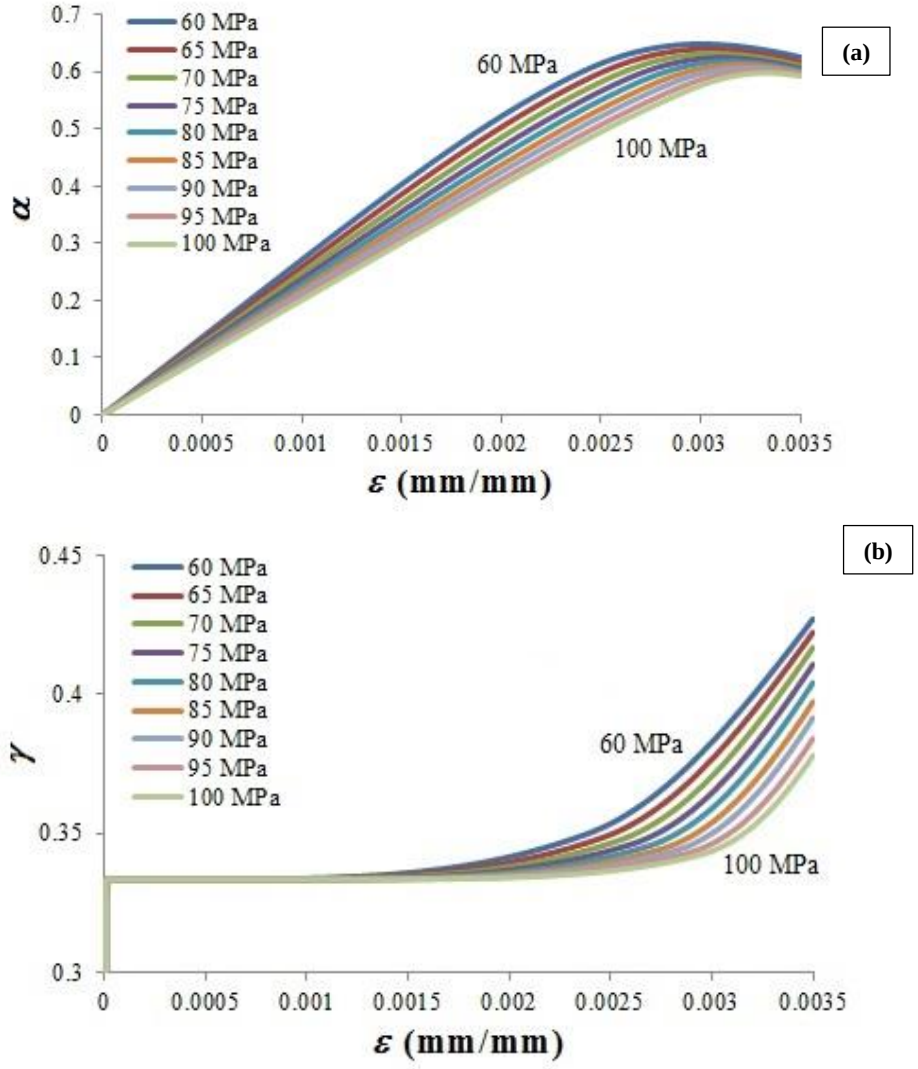

Figure 3. Parameters (a) α, (b) γ, against concrete strain in extreme compression fiber ε_c, for different HSC strengths

The rectangular stress block parameters proposed by some selected codes are given in Table 1 [29-32]. Based on recommendations of these building codes, when $\varepsilon_c = \varepsilon_{cu}$, one could easily estimate the width and height of equivalent stress block by $\alpha f_c'/2\gamma$, and $2\gamma c$, respectively.

Table 1. Rectangular stress block parameters of considered design codes

Ref.	$\alpha/2\gamma$	2γ	ε_{cu}
ACI 318 [30]	0.85	$1.09-0.008f_c'$ $0.65 \le 2\gamma \le 0.85$	0.003
Eurocode 2 [31]	$1.25-0.005f_c' \le 1.0$	$0.925-0.0025f_c' \le 0.8$	$0.0026+0.035(\frac{90-f_c'}{100})^4$ $0.0026 \le \varepsilon_{cu} \le 0.0035$
CSA A32.3 [29]	$0.67 \le 0.85-0.0015f_c'$	$0.67 \le 0.97-0.0025f_c'$	0.0035
NZS 3101 [32]	$1.07-0.004f_c'$ $0.75 \le \frac{\alpha}{2\gamma} \le 0.85$	(ACI 318)	0.003

Figure 4 a and b show the comparison of parameters $\alpha/2\gamma$ and 2γ, derived from the HSC stress-strain model described above, with parameters specified in ACI 318 [30], Eurocode 2 [31], CSA A23.3 [29], and NZS 3101 [32], for different HSC strengths, respectively. Results indicate that the proposed values of parameter $\alpha/2\gamma$, agree with ACI 318, recommended values; hence, for HSC, using $\alpha/2\gamma = 0.85$, seems to be rational. Also, the proposed values of parameter 2γ, having the same tendency as Eurocode 2, but of lower values for concrete strength up to 90 MPa.

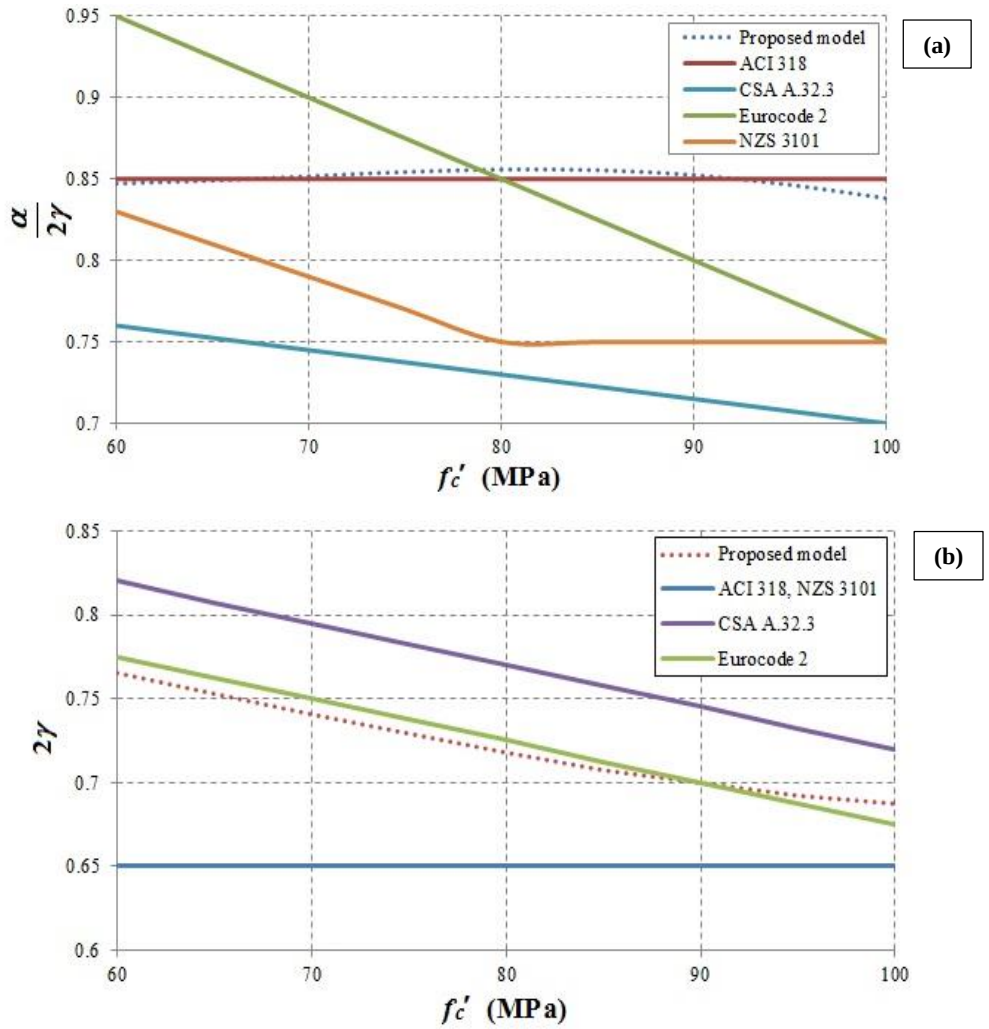

Figure 4. Equivalent stress block's parameters (a) $\frac{\alpha}{2\gamma}$, (b) 2γ, against HSC strength

2.2. Calculation of Resisting Moment and Curvature

By using an incremental deformation technique, strain and corresponding stress in the FRP composite, steel-reinforcement, and HSC, at any section are calculated [4]. Figure 1 shows the strain and corresponding stress/force diagrams for a typical rectangular RHSC beam-section with a FRP plate adhered to the tension face. As shown in Figure 5, based on the proposed algorithm, the strain in the extreme compressive fiber of HSC (ε_c) is increased until failure is reached. For different states, using the principle of strain compatibility, neutral axis location (c), is obtained from the equilibrium of internal forces. It must be noted that each of the internal force can be determined by multiplying stress by cross-sectional area.

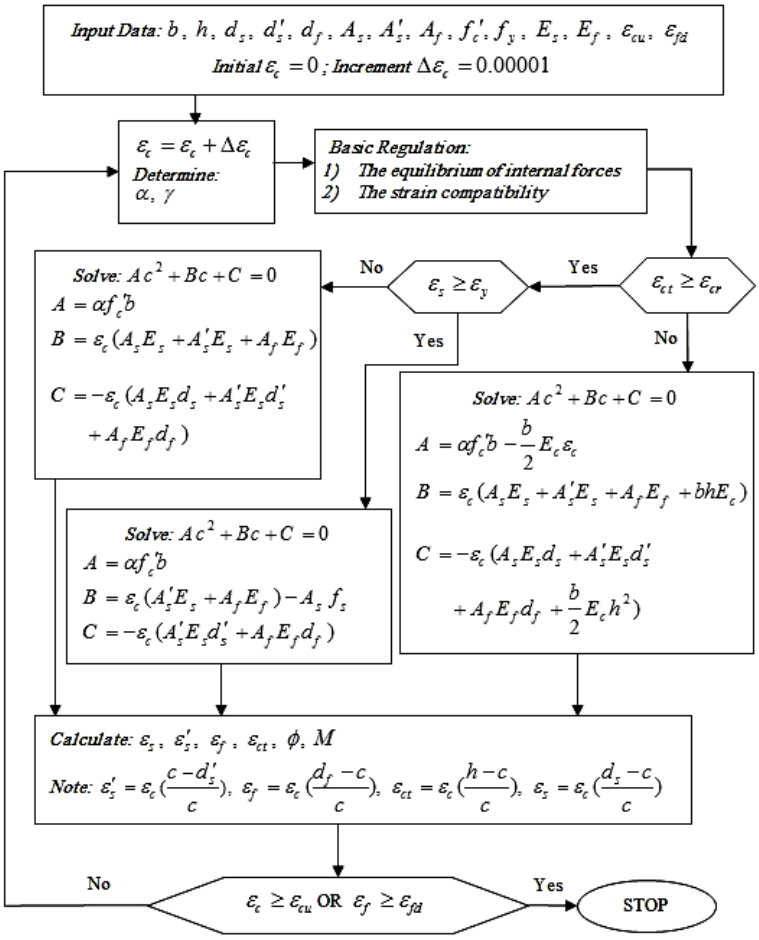

Figure 5. Algorithm of proposed analytical approach

The curvature is calculated by dividing the HSC strain ε_c by a distance to the neutral axis depth, C;

$$\phi = \frac{\varepsilon_c}{c} \tag{5}$$

The internal bending moment M of the section can be obtained by taking the sum of the moments (e.g. due to internal forces) about the neutral axis position. In this paper, due to use of the bilinear constitutive model for steel, one can calculate M as follows:

a) Before Cracking of HSC

$$M = \{\alpha f_c' b (1-\gamma) c^2 + A_s' E_s \varepsilon_s' (c - d_s') + A_s E_s \varepsilon_s (d_s - c) + A_f E_f \varepsilon_f (d_f - c) + \frac{1}{3} \varepsilon_{ct} E_c b (h-c)^2\} \tag{1-6}$$

b) After Cracking of HSC and before Yielding of Steel

$$M = \alpha f_c' b (1-\gamma) c^2 + A_s' E_s \varepsilon_s' (c - d_s') + A_s E_s \varepsilon_s (d_s - c) + A_f E_f \varepsilon_f (d_f - c) \tag{2-6}$$

C) After Yielding of Steel

$$M = \alpha f_c' b (1-\gamma) c^2 + A_s' E_s \varepsilon_s' (c - d_s') + A_s f_s (d_s - c) + A_f E_f \varepsilon_f (d_f - c) \tag{3-6}$$

3. Verification of the Proposed Analytical Model

3.1. Experimental Data

In order to verify the accuracy of the proposed analytical model, available experimental data on the flexural behavior of non-strengthened/FRP-strengthened RHSC beams are collected from the existing literature [4, 33-37]. The key parameters of these tested beams are summarized in Table 2. It must be noted that the compressive strength (f_c) of beams is varied from 54 to 126.2 MPa.

Akbarzadeh and Maghsoudi (2010), experimentally investigated the bending response of RHSC continuous (e.g. two-span) beams strengthened with externally-bonded CFRP and GFRP sheets along their negative (hogging) and positive (sagging) moment regions. The modulus of elasticity, yield strength and maximum tensile strength of steel rebar are 200 GPa, 412.5 MPa, and 626.4 MPa, respectively. The beams were loaded with a concentrated load at the middle of each span [4]. Hashemi et al. (2009) studied the flexural behavior of RHSC beams strengthened with FRP sheets under four-point bending test [33]. Maghsoudi and Akbarzadeh (2006), and also Rashid and Mansur (2005) have tested RHSC beams under four-point bending test [34-35]. Rabinovitch and Frostig (2003) experimentally investigated flexural response of RHSC beams strengthened and rehabilitated with externally-bonded CFRP strips using four-point bending test [36]. Rahimi and Hutchinson (2001) assessed the structural behavior of reinforced concrete beams strengthened with adhesively bonded fiber reinforced plastics (CFRP and GFRP) by four-point flexural testing of 2.3-m-long beams [37].

3.2. Results

The proposed analytical model was applied to obtain nonlinear moment–curvature curves at the central support/mid-span sections as the critical sections of tested beams. The comparison between experimental and predicted moment at the critical sections including the mode of failure are presented in Table 3. The comparison of results indicated that a very good accuracy of the proposed model is approached by -1.27 % mean value of errors. Also, the proposed analytical model can predict very well the experimental failure mode.

Some selected analytical and experimental moment–curvature responses of database beams (tests CB and SC1 of [4]) are shown in Figure 6 and 7. Same as the experimental responses, the three zones of pre-cracking, post-cracking pre-yield and post-yield zones were observed in the simulation results. Considering moment–curvature response, failure moment and failure mode, the comparison of results indicates that, the proposed model agrees very well with the experimental results.

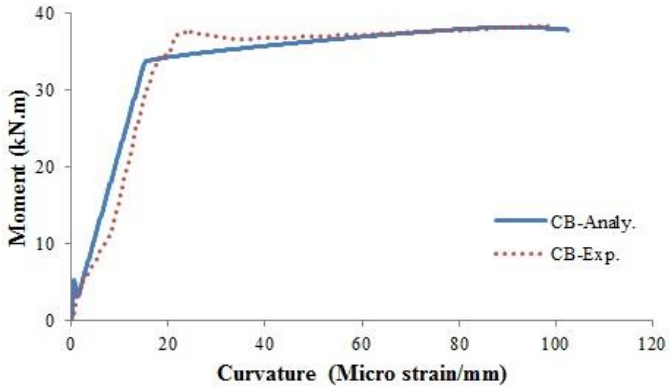

Figure 6. Analytical versus experimental moment–curvature response for beam CB

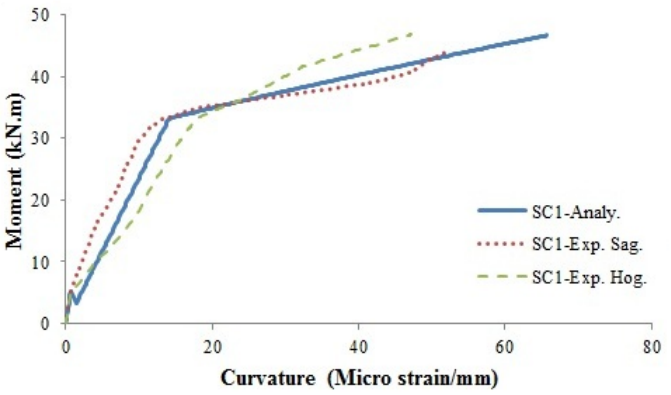

Figure 7. Analytical versus experimental moment–curvature response for beam SC1

Table 2. Details of the test specimens

Beam No.	Ref.	f_c (MPa)	b (mm)	h (mm)	L (mm)	Main longitudinal steel		FRP reinforcement						
						Top	Bottom	Type	No. of layers	Arrangement	t_f (mm)	b_f (mm)	E_f (GPa)	ε_{fu} (%)
CB	[4]	74.2	150	250	6000	2Φ16	2Φ16	-	0	-	-	-	-	-
SC1		74.6				2Φ16	2Φ16	CFRP	1	Positive and negative moment regions	0.11	145	242	1.55
SC2		74.1				2Φ16	2Φ16	CFRP	2	Positive and negative moment regions	0.11	145	242	1.55
SC3		74.4				2Φ16	2Φ16	CFRP	3	Positive and negative moment regions	0.11	145	242	1.55
SG3		79.7				2Φ16	2Φ16	GFRP	3	Positive and negative moment regions	0.2	145	73	3.1
AH0	[33]	77	150	250	3000	2Φ10	2Φ16	-	0	-	-	-	-	-
AH1						2Φ10	2Φ16	CFRP	1	Mid-span	0.045	150	230	1.67
BH0						2Φ10	2Φ22	-	0	-	-	-	-	-
BH1						2Φ10	2Φ22	CFRP	1	Mid-span	0.045	150	230	1.67
B1	[34]	65	200	300	2000	-	2Φ14	-	0	-	-	-	-	-
B2		65				-	2Φ20	-	0	-	-	-	-	-
B3		70				-	4Φ18	-	0	-	-	-	-	-
B4		70				-	4Φ20	-	0	-	-	-	-	-
D211	[35]	114.5	250	400	3600	2Φ13	4Φ25	-	0	-	-	-	-	-
E211		126.2				2Φ13	4Φ25	-	0	-	-	-	-	-
B211a		73.6				2Φ13	4Φ25	-	0	-	-	-	-	-
A1	[36]	75.3	200	200	2500	2Φ8	3Φ12	-	0	-	-	-	-	-
A2						2Φ8	3Φ12	CFRP	1	Mid-span	1.2	120	165	1.7
B-0.0	[37]	54-69	200	150	2300	2Φ10	2Φ10	-	0	-	-	-	-	-
B-0.4						2Φ10	2Φ10	CFRP	2	Mid-span	0.4*	150	127	1.21
B-1.8						2Φ10	2Φ10	GFRP	12	Mid-span	1.8*	150	36	3.1

* Total thickness of FRP reinforcement.

Table 3. Comparisons between experimental and predicted moment

Beam No.	Ref.	Experimental failure moment (kN.m)		Analytical failure moment (kN.m)		Failure mode**		Error (%)	
		Central support	Mid-span	Central support	Mid-span	Analytical model	Experimental observation	Central support	Mid span
CB	[4]	36.33	39.54	37.85	37.85	CC	CC	4.18	-4.27
SC1		46.74	44.53	46.68	46.68	FR	FR	-0.13	4.83
SC2		56.50	49.87	58.68	48.90	FD/FR	FD/FR	3.86	-1.95
SC3		68.26	58.14	66.60	55.50	FD	FD	-2.43	-4.54
SG3		57.20	50.72	59.89	49.91	FD	FD	4.70	-1.60
AH0	[33]	-	36.57	-	36.77	CC	CC	-	0.55
AH1		-	40.45	-	40.44	FR	FR	-	-0.02
BH0		-	69.23	-	64.59	CC	CC	-	-6.70
BH1			67.51		67.36	FR	FR		0.22
B1	[34]	-	36.93	-	30.48	CC	CC	-	-17.47
B2		-	74.74	-	65.08	CC	CC	-	-12.92
B3		-	80.00	-	88.99	CC	CC	-	11.24
B4		-	122.28	-	119.28	CC	CC	-	-2.45
D211	[35]	-	363.00	-	353.63	CC	CC	-	-2.58
E211		-	357.12	-	352.23	CC	CC	-	-1.37
B211a		-	300.54	-	295.34	CC	CC	-	-1.73
A1*	[36]	-	26.42	-	26.10	-	-	-	-1.21
A2		-	54.81	-	52.32	FD	FD	-	-4.54
B-0.0	[37]	-	10.80	-	11.00	CC	CC	-	1.85
B 0.4			20.19		18.95	FD	FD		6.14
B-1.8		-	22.63	-	24.43	FD	FD	-	7.95

*Loading was stopped at a deflection of about 50 mm.

**CC: Concrete Crushing; FR: FRP Rupture; FD: FRP Debonding.

4. Derivation of Proposed Formulas for Bending Ductility Indices

4.1. Parametric Study

The ductility of a structural member may be defined as its ability to deform up to the failure load without a significant loss in its load-carrying capacity. In seismic areas, ductility is an important factor in design of RC members under flexure [14]. Since some experimentally observed failure mechanisms in FRP-strengthened members are abrupt and brittle, and by considering HSC as a brittle material, therefore, understanding the effect of such materials (e.g. HSC and FRP) on the ductility of RC flexural members (e.g. beams) is notable. Several forms of ductility are often considered; these include curvature, rotational, displacement and energy ductility. In this research, curvature ductility and flexural energy ductility indices as the forms of bending ductility are investigated. Curvature ductility index can be calculated as defined by Equation 7.

$$\mu_{\phi} = \frac{\phi_u}{\phi_y} \tag{7}$$

In order to investigate the effects of concrete strength, steel-reinforcement ratio and externally-reinforcement (FRP) stiffness on the flexural behavior and the curvature ductility index of the FRP-strengthened RHSC beams; a parametric study is conducted for a typical beam section (Figure 1) with $b = 200$ mm (width), and $h = 400$ mm (total depth). For the aforementioned purposes, the cylindrical compressive strength of HSC f_c' is varied from 60 to 100 MPa, the yield strength of reinforcing steel $f_y = 400$ MPa and Young's modulus of reinforcement steel $E_s = 200$ GPa. The tension reinforcement ratio $\rho(\rho = A_s/bd)$ is varied from 10 to 100% of the balanced reinforcement ratio ρ_b of RHSC sections which are calculated by Equation 8, and listed in Table 4.

$$\rho_b = \alpha \frac{f_c'}{f_y}\left(\frac{700}{700 + f_y}\right) \tag{8}$$

Table 4. Balanced reinforcement ratios for different HSC strengths

Type	Compressive strength of HSC f_c' (MPa)				
	60	**70**	**80**	**90**	**100**
Balanced reinforcement ratio (ρ_b)	0.059	0.066	0.072	0.080	0.088

The tension reinforcement is provided at depth $d = 340$ mm from the top. Also the externally-reinforcement (FRP) stiffness K ($K = E_f A_f$) is varied from 5000 to 20000 GPa.mm^2. FRP plate's width and FRP rupture strain are assumed 200 mm and 1.5%, respectively.

The theoretical moment and curvature for FRP-strengthened RHSC beams sections are calculated by using the analytical proposed model. Figure 8 shows some analytical moment-curvature responses of strengthened beam sections with concrete strength $f_c' = 80$ MPa, FRP stiffness $K = 5000$ GPa.mm^2 and different tension reinforcement ratio (ρ). Comparing theses curves for different steel ratio, it can be seen that the tension reinforcement ratio basically affects both the shape of moment-curvature curve and the ductility of a beam section; as increasing the tension reinforcement ratio, the plateau of curve at the post-peak stage becomes gradually shorter and drops more rapidly that indicating remarkable reduction in ductility.

Figure 9 shows some selected moment-curvature responses of FRP-strengthened RHSC beam sections with concrete strength $f_c' = 80$ MPa and tension reinforcement ratio $\rho = 0.5\rho_b$ for different FRP stiffness (K). The increase of FRP stiffness leads to increase of the failure moment and post-yield stiffness and also decrease the ultimate curvature but the curvature at yielding load remains almost constant.

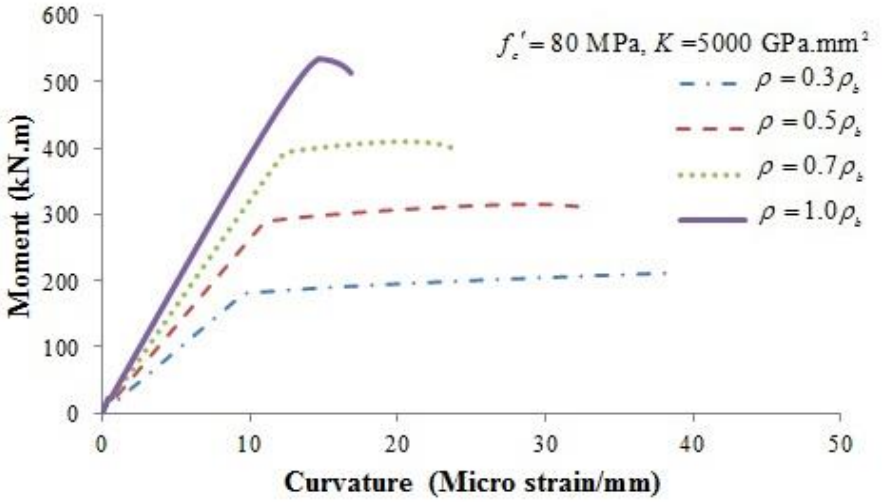

Figure 8. Analytical moment–curvature response for FRP strengthened RHSC beam sections with different steel ratio

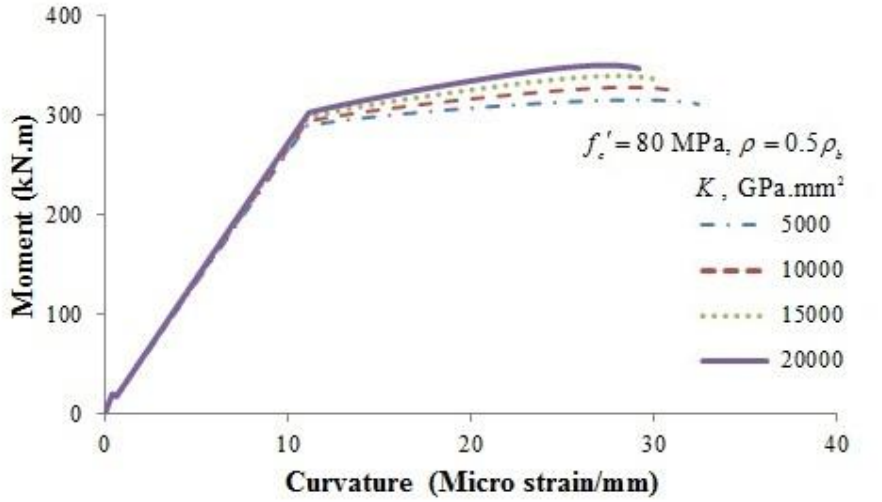

Figure 9. Analytical moment–curvature response for FRP strengthened RHSC beam sections with different FRP stiffness

The curvature ductility index μ_ϕ of FRP-strengthened RHSC beam section is calculated by, Equation 7. Figure 10 shows a plot of curvature ductility index as a function of steel-reinforcement ratio for FRP-strengthened RHSC beam sections with FRP stiffness $K = 10000$ GPa.mm^2 and different HSC strengths. The curvature ductility index decreases with increasing steel-reinforcement ratio.

Figure 11 shows a plot of curvature ductility index as a function of FRP stiffness for FRP-strengthened RHSC beam sections with steel-reinforcement ratio $\rho = 0.6\rho_b$ and different HSC strengths. It indicates that the curvature ductility index decreases with an increase in FRP stiffness.

Figure 12 shows a plot of curvature ductility index as a function of HSC strength for FRP-strengthened RHSC beam sections with steel-reinforcement ratio $\rho = 0.5\rho_b$ and different FRP stiffness. The curvature ductility index increases with an increase in HSC strength, but up to a certain level of concrete strength, about 90 MPa; beyond this level, the curvature ductility index slightly decreases as the HSC strength is increased.

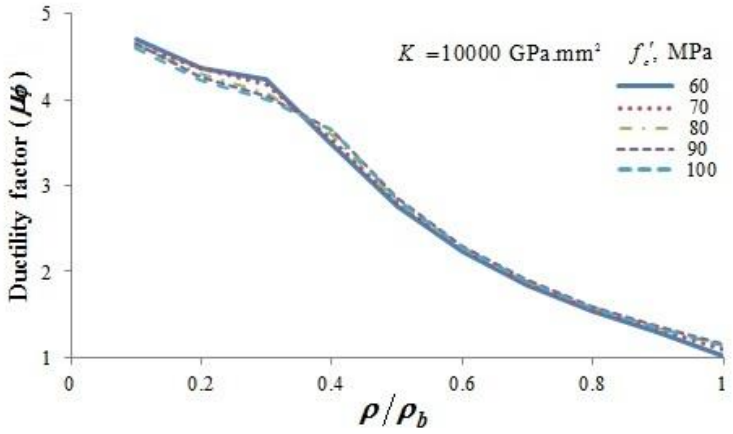

Figure 10. Ductility factor of FRP strengthened RHSC beam sections against amount of steel-reinforcement

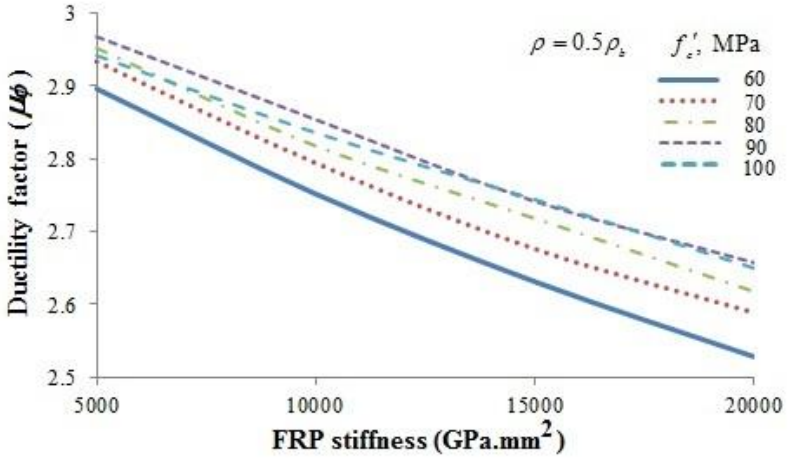

Figure 11. Ductility factor of FRP strengthened RHSC beam sections against FRP stiffness

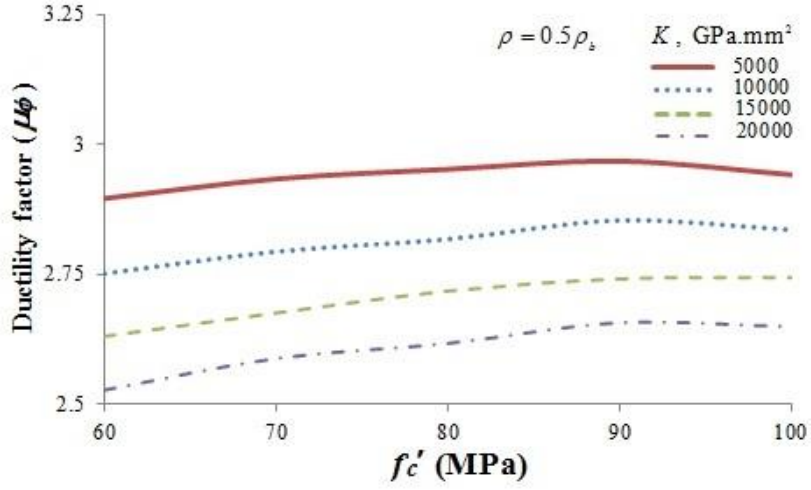

Figure 12. Ductility factor of FRP strengthened RHSC beam sections against HSC strength

4.2. Proposed Curvature Ductility Index Formula

According to the aforementioned analytical results, it is estimated that the HSC strength (f_c'), the amount of steel-reinforcement (ρ/ρ_b), and FRP stiffness (K), have influence on the curvature ductility index of FRP-strengthened RHSC beam sections. Thus, the basic formation of the curvature ductility index equation for FRP-strengthened RHSC beam sections can be expressed as defined by Equation 9.

$$\mu_\phi = f\ (f_c',\ \rho/\rho_b,\ K) = f_1(\rho/\rho_b).f_2(K).f_3(f_c') \tag{9}$$

Also based on the analytical results described previously, the curvature ductility index and the amount of steel-reinforcement, FRP stiffness and HSC strength are mutually related with f_i, as the 2nd-order polynomial, 3rd-order

polynomial and exponential function, respectively. So the prediction equation of the curvature ductility index for FRP-strengthened RHSC beam sections can be expressed as following:

$$\mu_\phi = f_1(\rho/\rho_b).f_2(K).f_3(f_c') = (a_1\{a_2(\rho/\rho_b)^3 + a_3(\rho/\rho_b)^2 + a_4(\rho/\rho_b) + a_5\} \times (K)^{a_6} \times \{a_7(f_c')^2 + a_8(f_c') + a_9\}) \quad (10)$$

Where the coefficient a_i are determined from multiple regression analysis, which is using the analytical results [16]. Figure 13 shows the relationship of the curvature ductility index and parameter ρ/ρ_b which can be obtained by regression analysis on the analytical results as follows:

$$\mu_\phi = \{7.698(\rho/\rho_b)^3 - 11.564(\rho/\rho_b)^2 + 0.466(\rho/\rho_b) + 4.572\} \quad (11)$$

The analytical results indicate that the curvature ductility index decrease with increasing of FRP stiffness. By regression analysis, the relationship between the ratio $\mu_\phi/f_1(\rho/\rho_b)$ and the FRP stiffness which is shown in Figure 14, can be obtained as follows:

$$\mu_\phi/f_1(\rho/\rho_b) = 1.702(K)^{-0.057} \quad (12)$$

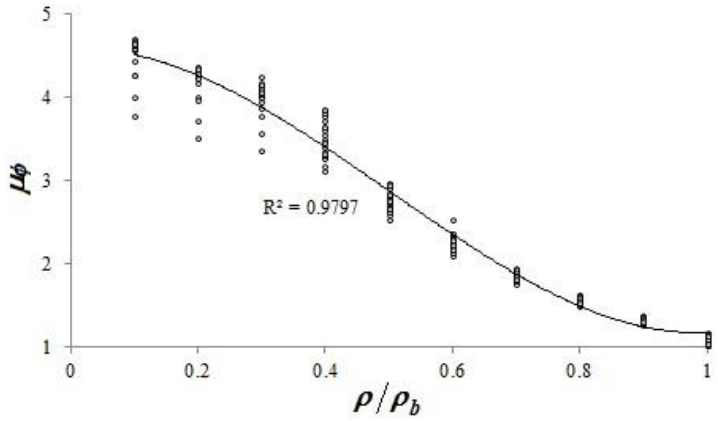

Figure 13. Influence of parameter ρ/ρ_b on the curvature ductility factor

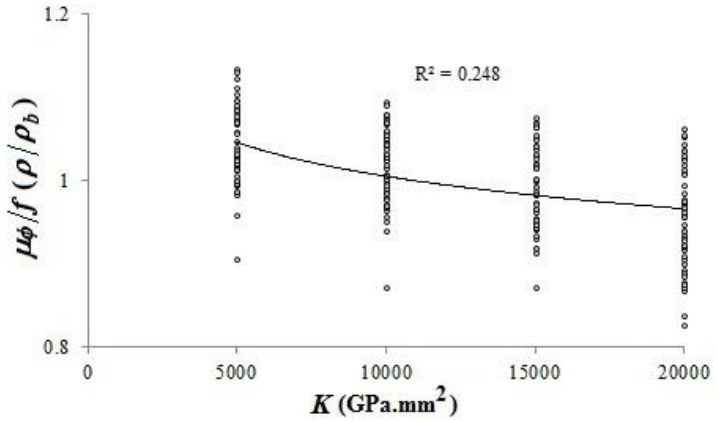

Figure 14. Influence of FRP stiffness on the ratio of μ_ϕ to $f_1(\rho/\rho_b)$

The effect of HSC strength on the ratio of the curvature ductility index to $f_1(\rho/\rho_b) \times f_2(K)$ is shown in Figure 15. By regression analysis, the relationship between these parameters can be expressed as follows:

$$\mu_\phi/\{f_1(\rho/\rho_b) \times f_2(K)\} = \{-8.0 \times 10^{-5}(f_c')^2 + 0.014(f_c') + 1.087\} \quad (13)$$

Finally, the prediction equation of curvature ductility index can be offered based on the parametric study as follows:

$$\mu_\phi = (\{7.698(\rho/\rho_b)^3 - 11.564(\rho/\rho_b)^2 + 0.466(\rho/\rho_b) + 4.572\} \times (K)^{-0.057} \times \{-8.0 \times 10^{-5}(f_c')^2 + 0.014(f_c') + 1.087\}) \quad (14)$$

Figure 16 shows the comparison of the proposed curvature ductility index obtained by Equation 14 with the analytical

results. The proposed predictions show excellent agreement as evident from coefficients correlation R^2 well above 0.98 and the mean error is 1.87%, so the proposed equation is accurate enough for practical applications.

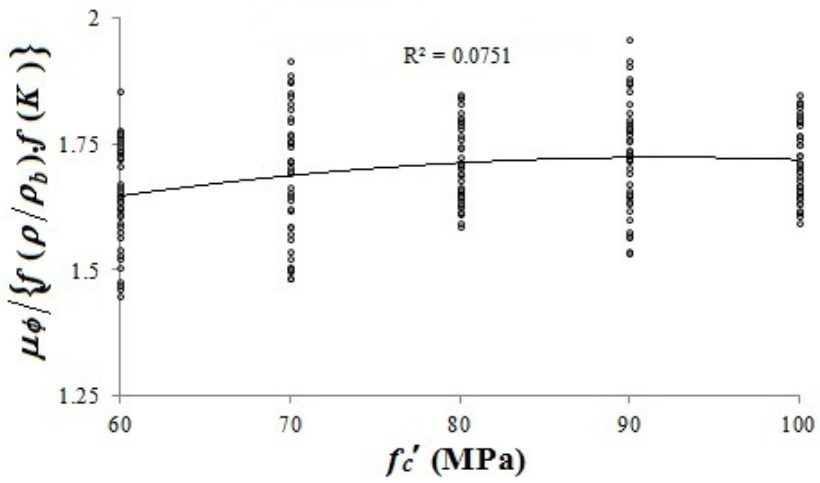

Figure 15. Influence of HSC strength on the ratio of μ_ϕ to $f_1(\rho/\rho_b)\times f_2(K)$

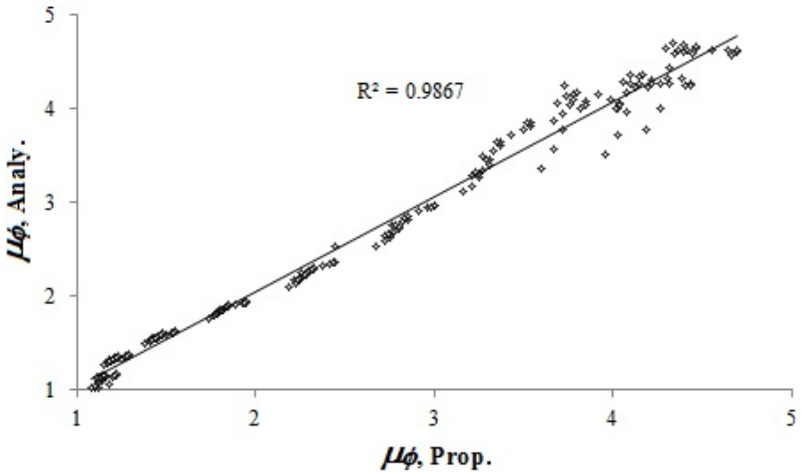

Figure 16. Performance of proposed formula in predicting μ_ϕ

4.3. Proposed Energy Ductility Index Formula

Another method of determining bending ductility is based on the energy definition which is illustrated in Figure 17. As defined by Equation 15, energy ductility index can be calculated as the ratio between the flexural energy of the system at failure, E_u , and the flexural energy of the system at first yielding of tensile steel, E_y .

$$\mu_E = \frac{E_u}{E_y} \tag{15}$$

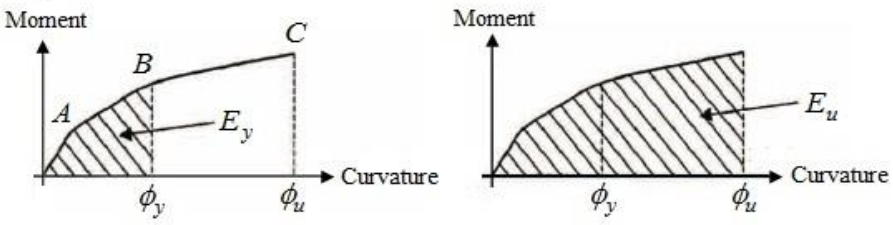

Figure 17. Definition of energy ductility index, μ_E

By using the aforementioned analytical moment-curvature responses, and Equation 15, the energy ductility index, μ_E , of FRP-strengthened RHSC beam section is calculated. As shown in Figure 18, the relationship of the curvature ductility index, μ_ϕ , and energy one, μ_E , can be expressed as defined in Equation 16.

$$\mu_E = 1.0826(\mu_\phi)^{1.4582} \quad (16)$$

By using Equation 14, for μ_ϕ in Equation 16, as shown in Figure 19, the comparison of the proposed energy ductility index with the analytical results is presented. The proposed predictions show excellent agreement as evident from coefficients correlation R^2 well above 0.97 and the mean error is 3.03%, so the proposed equation is accurate enough for practical applications.

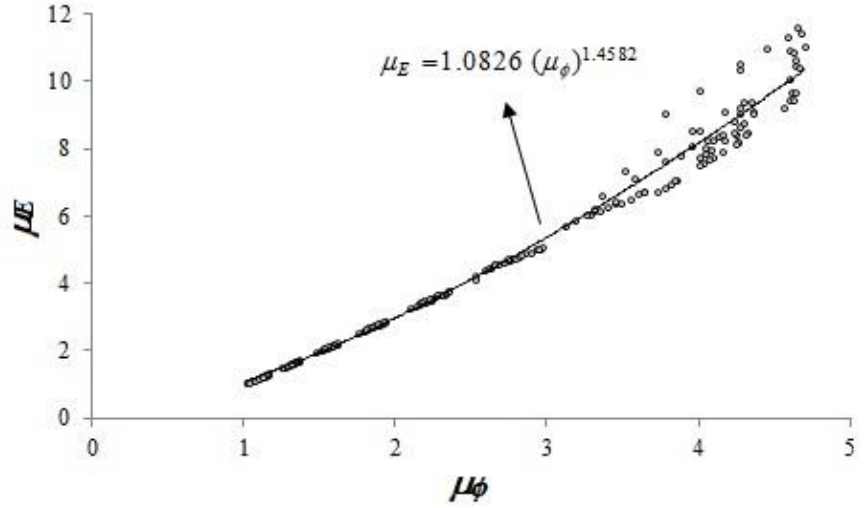

Figure 18. Relationship of bending ductility indices of μ_ϕ and μ_E

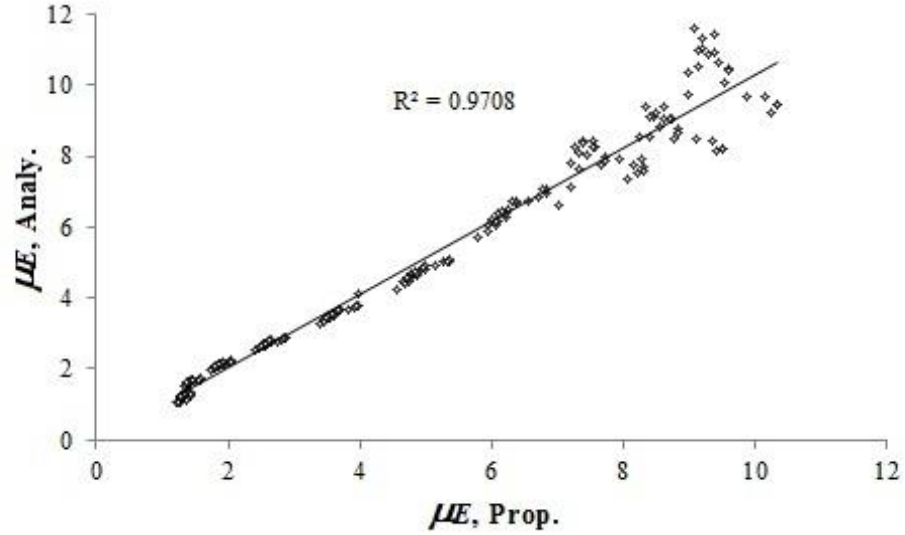

Figure 19. Performance of proposed formula in predicting μ_E

5. Derivation of Limit Values based on Design Codes

Design codes prescribe some limiting constraints to ensure sections would possess adequate ductility. In most of the existing design codes, these constrains impose limits on either the tensile rebar strain or the neutral axis depth. Based on ACI 318, for the tension-controlled section, which is expected to failure in sufficiently ductile manner, a minimum limit value of 0.005 for the strain at foremost tensile rebar, ε_{st}, is recommended. Also, a minimum limit value of 0.0075 for ε_{st}, is suggested for moment redistribution in flexural continuous members, to ensure an adequate ductility in plastic hinge regions [30]. For ductile design, Eurocode 2, recommended that the neutral axis depth to effective depth ratio (c/d), should be limited to 0.35, for concrete grades higher than C35/45. Its limit on the c/d ratio could be transformed to the tensile rebar strain format; it means that by considering $\varepsilon_{cu} = 0.0035$, the limit value of ε_{st}, is 0.0065 [31].

Figure 20 and 21, show the relationship of bending ductility indices (μ_ϕ and μ_E), and ε_{st}, for FRP strengthened RHSC beam sections with different HSC strengths. Also, in these figures, ACI 318, tension control limit ($\varepsilon_{st} \geq 0.005$), reinforcement strain limit, which has used in the definition of maximum reinforcement ratio, ρ_{max} ($\varepsilon_{st} \geq 0.004$), and compression control limit ($\varepsilon_{st} \leq \varepsilon_y$), are plotted.

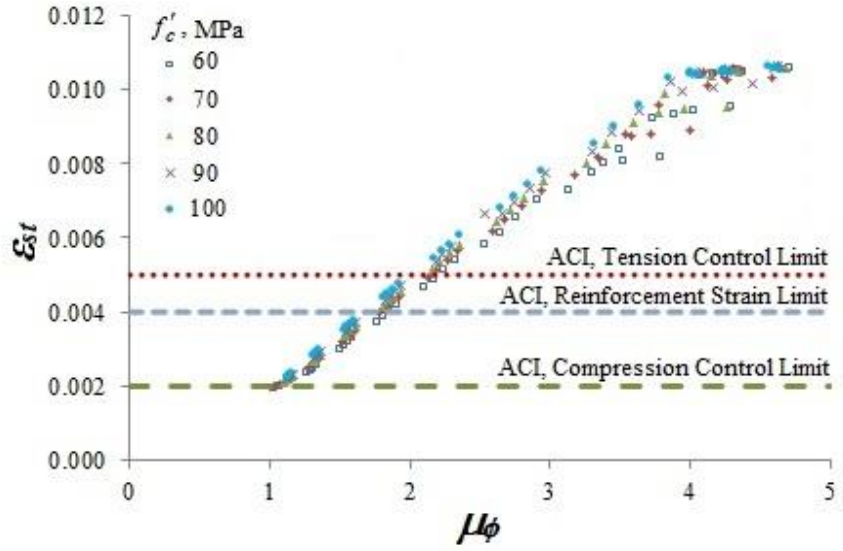

Figure 20. Relationship of curvature ductility index and the strain at foremost tensile rebar ε_{st} , for different HSC strengths

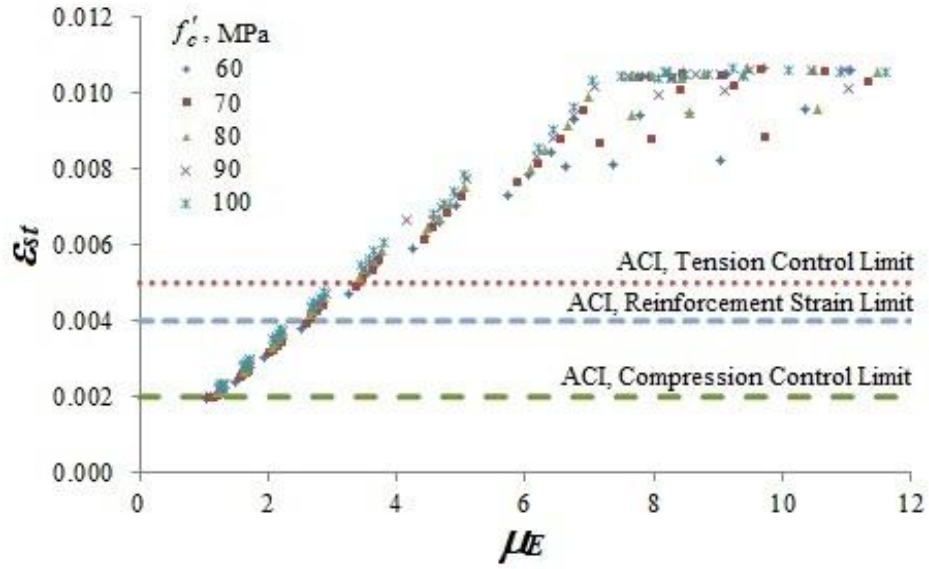

Figure 21. Relationship of energy ductility index and the strain at foremost tensile rebar ε_{st} , for different HSC strengths

Results indicate that the minimum value of μ_ϕ and μ_E which satisfy ACI 318, tension control limit, are 2.16 and 3.43, respectively that belong to strengthened beam section with $f_c' = 80$ MPa , $\rho = 0.6\rho_b$, and $K = 20000$ GPa.mm^2. Table 5 showed the minimum values of μ_ϕ and μ_E , which satisfy ACI 318 and Eurocode 2, recommendations for the ductile manner.

Table 5. The minimum values of bending ductility indices based on ACI 318 and Eurrocode 2 recommendations

Ductility	Strain at foremost tensile rebar, ε_{st}		
	≥ 0.005	≥ 0.0065	≥ 0.0075
μ_ϕ	2.16	2.53	2.94
μ_E	3.43	4.14	5.06

These resulted values of μ_ϕ are about $2 \sim 4$ times lower than minimum ones recommended by the existing literature for seismic zones [14, 17]. To some extent, it seems compression and/or confining-reinforcement could make up the reduction in bending ductility indices [14]. Nevertheless, for strengthened members, which containing some brittle materials (e.g. HSC and FRP), it seems that the codes' recommendations (especially in seismic areas) need to be modified by using results of some extra experimental and analytical studies.

6. Conclusion

An iterative analytical technique has been presented which considers nonlinear behavior of materials. The analyses results show good agreement with the experimental data of non-strengthend and FRP strengthened RHSC beams, regarding moment–curvature response, ultimate moment, ductility and failure mode. The effects of HSC strength, steel-reinforcement ratio and FRP stiffness on flexural behavior and bending ductility indices of FRP strengthened RHSC beam sections have been studied and newly prediction formulas for curvature ductility index, μ_ϕ , and energy ductility index, μ_E , of FRP strengthened RHSC beam sections have been developed.

The curvature ductility index of FRP strengthened RHSC beam sections increases with an increase in HSC strength, but up to a certain level of concrete strength about 90 MPa and decreases with an increase of steel-reinforcement ratio and FRP stiffness, respectively.

Results indicate that the minimum value of μ_ϕ , and μ_E , which satisfy ACI 318, tension control limit, are 2.16, and 3.43, respectively.

Based on verifying the analytical results, the proposed predictions for the curvature ductility index and energy one are accurate to within 1.87%, and 3.03% error for practical applications, respectively. The proposed formulas offer fairly accurate and consistent predictions of bending ductility indices for FRP strengthened RHSC beam sections.

7. Notations

A_f	FRP reinforcement area
A_s	Tensile steel rebar area
A_s'	Compressive steel rebar area
a_i	Coefficient
b	Width of rectangular beam section
b_f	Width of FRP
c	Neutral axis depth
d_f	Distance from extreme compression fiber to centroid of FRP reinforcement
d_s	Effective depth of rectangular beam section
d_s'	Distance from extreme compression fiber to centroid of compressive steel rebar
E_c	Elastic modulus of concrete
E_f	Elastic modulus of FRP
E_s	Elastic modulus of steel
E_u	Ultimate flexural energy of the system
E_y	Yield flexural energy of the system
f , f_i	Function
f_c'	The cylindrical compressive strength of concrete
f_s	Stress in tensile steel rebar
f_u	Ultimate strength of steel rebar
f_y	Yield strength of steel rebar
h	Height of rectangular beam section
K	FRP stiffness
L	Length of beam
M	The internal bending moment
n_f	Number of FRP layers
t_f	Thickness of FRP per one layer
α, γ	Equivalent stress block parameters
ε_0	Concrete strain at peak stress
ε_c	Strain in the extreme compressive fiber of concrete
ε_{cu}	Concrete ultimate strain
ε_f	FRP strain

ε_{fd}	FRP debonding strain
ε_{fe}	FRP effective strain attained at failure
ε_{fu}	FRP design rupture strain
ε_s	Tensile steel rebar strain
ε_{st}	Strain at foremost tensile steel rebar
ε_s'	Compressive steel rebar strain
μ_E	Energy ductility index
μ_ϕ	Curvature ductility index
ρ	The tension reinforcement ratio
ρ_b	The balanced reinforcement ratio
ϕ	Curvature
ϕ_u	Ultimate curvature
ϕ_y	Yield curvature

8. Conflicts of Interest

The authors declare no conflict of interest.

9. References

[1] Rasheed, H.R. "Strengthening design of reinforced concrete with FRP" (2015). doi:10.1201/b17968.

[2] Teng, J.G., S.T. Smith, J. Yao, and J.F. Chen. "Intermediate crack-induced debonding in RC beams and slabs." Construction and Building Materials 17 (September 2003): 447-462. doi:10.1016/s0950-0618(03)00043-6.

[3] Ashour, A.F., S.A. El-Refaie, and S.W. Garrity. "Flexural strengthening of RC continuous beams using CFRP laminates." Cement and Concrete Composite 26 (October 2004): 765-775. doi:10.1016/j.cemconcomp.2003.07.002.

[4] Akbarzadeh, H., and A.A. Maghsoudi. "Experimental and analytical investigation of reinforced high strength concrete continuous beams strengthened with fiber reinforced polymer." Materials and Design 31 (March 2010): 1130-1147. doi:10.1016/j.matdes.2009.09.041.

[5] Akbarzadeh, H., and A.A. Maghsoudi. "Experimental investigations and verification of debonding strain of RHSC continuous beams strengthened in flexure with externally bonded FRPs." Materials and Structures 43 (2010): 815-837. doi:10.1617/s11527-009-9550-7.

[6] Cruz-Noguez, C.A., D.T. Lau, E.G. Sherwood, S. Hiotakis, J. Lombard, S. Foo and M. Cheung. "Seismic behavior of RC shear walls strengthened for in-plane bending using externally bonded FRP sheets." Journal of Composites for Construction (ASCE) 19 (1) (February 2015): 04014023. doi:10.1061/(asce)cc.1943-5614.0000478.

[7] Mostofinejad, D., and N. Moshiri. "Compressive strength of CFRP composites used for strengthening of RC columns: comparative evaluation of EBR and grooving methods." Journal of Composites for Construction (ASCE) 19 (5) (October 2015): 04014079. doi:10.1061/(asce)cc.1943-5614.0000545.

[8] Ghasemi, S., A.A. Maghsoudi, H. Akbarzadeh Bengar, and H.R. Ronagh. "Sagging and hogging stren gthening of continuous unbonded posttensioned HSC beams by NSM and EBR." Journal of Composites for Construction (ASCE) 20 (2) (April 2016): 04015056. doi:10.1061/(asce)cc.1943-5614.0000621.

[9] Qeshta, I.M.I., P. Shafigh, and M.Z. Jumaat. "Research progress on the flexural behaviour of externally bonded RC beams." Archives of Civil and Mechanical Engineering 16 (4) (September 2016): 982–1003. doi:10.1016/j.acme.2016.07.002.

[10] Mostofinejad, D., and A.R. Akhlaghi. "Experimental investigation of the efficacy of EBROG method in seismic rehabilitation of deficient reinforced concrete beam–column joints using CFRP sheets." Journal of Composites for Construction (ASCE) 21 (4) (August 2017): 04016116. doi:10.1061/(asce)cc.1943-5614.0000781.

[11] Oehlers, D.J. "Development of design rules for retrofitting by adhesive bonding or bolting either FRP or steel plates to RC beams or slabs in bridges and building." Composites: Part A 32 (September 2001): 1345-1355. doi:10.1016/s1359-835x(01)00089-6.

[12] ACI 363R. "State-of-the-art report on high-strength concrete." American Concrete Institute (2010).

[13] Rashid, M.A., M.A. Mansur, and P. Paramasivam. "Correlations between mechanical properties of high-strength concrete." Journal of Materials in Civil Engineering (ASCE) 14 (3) (June 2002): 230-238. doi:10.1061/(asce)0899-1561(2002)14:3(230).

[14] Maghsoudi, A.A. "Design for Ductility of Structures." Shahid Bahonar University Publications (1996) [in Persian].

[15] Maghsoudi, M., and A.A. Maghsoudi. "Moment redistribution and ductility of CFRP strengthened and non-strengthened unbonded post-tensioned indeterminate I-beams composed of UHSSCC." Composite Structures 174 (August 2017): 196–210. doi:10.1016/j.compstruct.2017.04.057.

[16] Lee, H.J. "Predictions of curvature ductility factor of doubly reinforced concrete beams with high strength materials." Computers and Concrete (An International Journal) 12 (6) (December 2013): 831-850. doi:10.12989/cac.2013.12.6.831.

[17] Lee, T., A.D.E Pan, and M.J.L. Ma. "Ductile design of reinforced concrete beams retrofitted with fiber reinforced polymer plates." Journal of Composites for Construction (ASCE) 8 (6) (December 2004): 489-500. doi:10.1061/(asce)1090-0268(2004)8:6(489).

[18] Matthys, S., and L. Taerwe. "Evaluation of ductility requirements in current design guidelines for FRP strengthening." Cement and Concrete Composites 28 (10) (November 2006): 845–856. doi:10.1016/j.cemconcomp.2006.07.003.

[19] Yost, J.R., and R.E. Steffen. "Strength and ductility trends for concrete members strengthened in flexure with carbon fiber-reinforced polymer reinforcement." Journal of Composites for Construction (ASCE) 18 (6) (December 2014): 04014015. doi:10.1061/(asce)cc.1943-5614.0000460.

[20] Teng, J.G., J.F. Chen, S.T. Smith, and L. Lam. "FRP strengthened RC structures" (2002).

[21] An, W., H. Saadatmanesh, and M.R. Ehsani. "RC beams strengthened with FRP plates - Part II: analysis and parametric study." Journal of Structural Engineering (ASCE) 117 (11) (November 1991): 3434–3455. doi:10.1061/(asce)0733-9445(1991)117:11(3434).

[22] El-Mihilmy, M.T. , and J.W. Tedesco. "Analysis of reinforced concrete beams strengthened with FRP laminates." Journal of Structural Engineering (ASCE) 126 (6) (June 2000): 684–691. doi:10.1061/(asce)0733-9445(2000)126:6(684).

[23] Toutanji, H., L. Zhao, and Y. Zhang. "Flexural behavior of reinforced concrete beams externally strengthened with CFRP sheets bonded with an inorganic matrix." Engineering Structures 28 (March 2006): 557–566. doi:10.1016/j.engstruct.2005.09.011.

[24] Skuturna, T., and J. Valivonis. "The statistical evaluation of design methods of the load-carrying capacity of flexural reinforced concrete elements strengthened with FRP." Archives of Civil and Mechanical Engineering 15 (1) (January 2015): 214–222. doi:10.1016/j.acme.2014.04.005.

[25] ACI 440.2R. "Guide for the design and construction of externally bonded FRP systems for strengthening concrete structures." American Concrete Institute (2017).

[26] Thorenfeldt, E., A. Tomaszewicz, and J.J. Jensen. "Mechanical properties of high strength concrete and application in design." Proceedings of the Symposium on Utilization of High Strength Concrete (1987).

[27] Popovics, S. "A numerical approach to the complete stress-strain curve of concrete." Cement and Concrete Research 3 (5) (September 1973): 583–599. doi:10.1016/0008-8846(73)90096-3.

[28] Collins, M.P., and A. Porasz. "Shear design for high-strength concrete." Comité Euro-International du Béton, Bulletin d'Information 193 (1989): 77-83.

[29] CSA A23.3. "Design of concrete structures." Canadian Standards Association (2004).

[30] ACI 318. "Building code requirements for structural concrete and commentary." American Concrete Institute (2014).

[31] Eurocode 2. "Design of concrete structures-Part 1: General rules and rules for Buildings." European Committee for Standardization (2004).

[32] NZS 3101. "Concrete structures standard–Part 1: The design of concrete structures." Standards New Zealand (2006).

[33] Hashemi, S.H., A.A. Maghsoudi, and R. Rahgozar. "Bending response of HSRC beams strengthened with FRP sheets." Scientia Iranica: Transaction A 16 (2) (2009): 138-146.

[34] Maghsoudi, A.A., and H. Akbarzadeh. "Flexural ductility of HSC members." Structural Engineering and Mechanics (An International Journal) 24 (2) (September 2006): 195-212. doi:10.12989/sem.2006.24.2.195.

[35] Rashid, M.A., and M.A. Mansur. "Reinforced high-strength concrete beams in flexure." ACI Structural Journal 102 (3) (2005): 462-471. doi:10.14359/14418.

[36] Rabinovitch, O., and Y. Frostig. "Experiments and analytical comparison of RC beams strengthened with CFRP composites." Composites: Part B 34 (December 2003): 663-677. doi:10.1016/s1359-8368(03)00090-8.

[37] Rahimi, H., and A. Hutchinson. "Concrete beams strengthened with externally bonded FRP plates." Journal of Composites for Construction (ASCE) 5 (1) (February 2001): 44-56. doi:10.1061/(asce)1090-0268(2001)5:1(44).